Electron transport in a ferromagnet-superconductor junction on graphene

Yasuhiro Asano,[1] Toshihiro Yoshida,[1] Yukio Tanaka,[2] and Alexander A. Golubov[3]
[1]*Department of Applied Physics, Hokkaido University, Sapporo 060-8628, Japan*
[2]*CREST-JST and Department of Applied Physics, Nagoya University, Nagoya 464-8603, Japan*
[3]*Faculty of Science and Technology, University of Twente, 7500 AE, Enschede, The Netherlands*
(Received 13 March 2008; revised manuscript received 16 June 2008; published 18 July 2008)

In a usual ferromagnet connected with a superconductor, the exchange potential suppresses the superconducting pairing correlation. We show that this common knowledge does not hold in a ferromagnet-superconductor junction on a graphene. When the chemical potential of a graphene is close to the conical point of energy dispersion, the exchange potential rather assists the charge transport through a junction interface. The loose-bottomed electric structure causes this unusual effect.

DOI: 10.1103/PhysRevB.78.014514 PACS number(s): 74.50.+r, 74.25.Fy, 74.70.Tx

I. INTRODUCTION

A long time ago Fulde-Ferrell[1] and Larkin-Ovchinnikov[2] have showed that superconducting order parameter becomes inhomogeneous under the action of an exchange potential. Such a superconducting state is called Fulde-Ferrell-Larkin-Ovchinnikov (FFLO) state and is currently a hot topic in condensed matter physics. A spin-singlet Cooper pair consists of two electrons with momenta $\boldsymbol{k}$ and $-\boldsymbol{k}$ on the Fermi surface. The exchange potential shifts such momenta to $\boldsymbol{k}+\boldsymbol{q}/2$ and $-\boldsymbol{k}+\boldsymbol{q}/2$ due to Zeeman effect. As a consequence, a Cooper pair acquires a center-of-mass momentum $\boldsymbol{q}$ and the superconducting order parameter oscillates in real space such as $\cos(\boldsymbol{q}\cdot\boldsymbol{r})$. Essentially similar effect has been predicted and observed in ferromagnet-superconductor (FS) and superconductor-ferromagnet-superconductor (SFS) proximity structures.[3–7] In metallic SFS junctions, the proximity effect in a ferromagnet causes unusual Josephson coupling. An SFS junction undergoes a transition from 0 state to π state as temperatures or length of a ferromagnet change because the pairing function in a ferromagnet changes its sign almost periodically as a function of spatial coordinate. In metallic FS junctions, the exchange potential V_{ex} suppresses the Andreev reflection.[8] Therefore the conductance of an FS junction decreases with the increase in V_{ex} and vanishes at $V_{\mathrm{ex}}=\mu$, where μ is the Fermi energy in the absence of exchange potential. For $V_{\mathrm{ex}}>\mu$, a ferromagnet becomes half metallic and the usual proximity effect is impossible in a ferromagnet.[9–13] This picture is valid when the minority spin conduction band has its bottom. Thus the above picture would be changed for the loose-bottomed band structure in graphene.

Graphene is a novel material attracting much attention recently. Carbon atoms on graphene are separated into two sublattices (A and B) due to its honeycomb lattice structure. In undoped graphene, the Fermi level lies on the conical point of the linear dispersion relation. In slightly doped graphene, two independent valleys appear on the Fermi surface. A considerable number of theoretical studies are made on transport properties of graphene because electronic structures can be described by the massless Dirac Hamiltonian.[14] The superconducting graphene junction was first discussed by Beenakker.[15] When the Fermi level in normal graphene is smaller than the pair potential of superconducting graphene, the Andreev reflection has the specular reflection property instead of the usual retroreflection. As a result, an electron-hole pair in the normal segment loses its retroreflection property even in the presence of time-reversal symmetry. Thus an unusual electronic transport is expected in superconducting graphene junctions.[16]

In this paper, we discuss electric current in FS and SFS junctions on graphene. When the exchange potential is much larger than the Fermi energy (i.e., $V_{\mathrm{ex}}\gg\mu$) in a ferromagnetic segment, the Andreev reflection always has the specular reflection property. As a consequence, the conductance spectra of FS junction become insensitive to V_{ex}. In addition, very small shot noise is expected because the Andreev reflection probability is unity at the zero bias irrespective of V_{ex}. In SFS junctions, the amplitude of Josephson current increases with increasing V_{ex}. In all cases, the exchange potential assists electron transport in graphene, in contrast to usual FS and SFS junctions.

II. CONDUCTANCE IN FS JUNCTIONS

Let us consider a graphene sheet on an insulator-superconductor junction as shown in Fig. 1(a), where the width of graphene sheet is W. There are several ways to

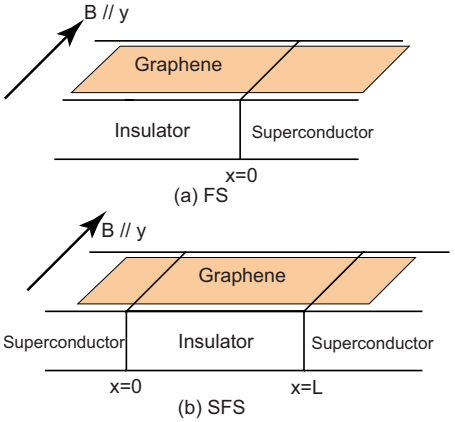

FIG. 1. (Color online) Schematic figures of FS and SFS junctions on graphene. The width of graphene is W.

introduce the exchange potential onto a ferromagnetic segment of graphene. Several theories suggested intrinsic ferromagnetic correlations.[17,18] It is also possible to substitute the insulator by a ferromagnetic insulator such as EuO.[19] A rough estimation[20] indicates the exchange splitting on graphene would be 5 meV. Although the Zeeman splitting due to external magnetic field is not large (1 meV per 20 T),[20] magnetic field in the y direction can tune the exchange splitting. In addition to these, a recent paper suggested the spin field-effect transistor using graphene[21] and the spin injection into graphene.[22] Thus introducing spin imbalance on graphene would be possible by combination of conventional technique or novel ideas of spin control. A junction on graphene is described by the Dirac-Bogoliubov–de Gennes equation[15]

$$\begin{bmatrix} \hat{h}_0 - sV_{\rm ex}\hat{\sigma}_0 & s\Delta(x)\hat{\sigma}_0 \\ s\Delta(x)^*\hat{\sigma}_0 & -\hat{h}_0 - sV_{\rm ex}\hat{\sigma}_0 \end{bmatrix} \Phi_s(\boldsymbol{r}) = E\Phi_s(\boldsymbol{r}), \tag{1}$$

$$\hat{h}_0 = -i\hbar v_F \nabla \cdot \hat{\boldsymbol{\sigma}} - [\mu + V(x)]\hat{\sigma}_0, \tag{2}$$

$$V(x) = \begin{cases} 0 & :x < 0 \\ -U_0 & :x > 0 \end{cases}, \tag{3}$$

$$\Delta(x) = \Delta e^{i\varphi}\Theta(x), \tag{4}$$

$$\Phi_s = \begin{bmatrix} \boldsymbol{u}_s \\ \boldsymbol{v}_s \end{bmatrix}, \quad \boldsymbol{u}_s(\boldsymbol{r}) = \begin{bmatrix} u_A^s \\ u_B^s \end{bmatrix}, \quad \boldsymbol{v}_s(\boldsymbol{r}) = \begin{bmatrix} v_A^s \\ v_B^s \end{bmatrix}, \tag{5}$$

where $\nabla = (\partial_x, \partial_y)$, v_F is a constant velocity, $\Theta(x)$ is the step function, $\hat{\sigma}_0$ is the 2×2 unit matrix, σ_j for $j=1-3$ is the Pauli matrix representing sublattice space, and μ and V_{ex} are the chemical potential and the exchange potential of a ferromagnetic segment, respectively. Here and in what follows, we take the unit of $\hbar = k_B = 1$, where k_B is the Boltzmann constant. The spin degree of freedom of a quasiparticle is represented by $s = \pm 1$; $s=1$ indicates a subspace of spin-up electron and spin-down hole, and $s=-1$ indicates a subspace of spin-down electron and spin-up hole. In this paper, $\hat{\cdots}$ indicates a 2×2 matrix in sublattice space and $\check{\cdots}$ means a 4×4 matrix in Nambu $\times$ sublattice space. The amplitude of the pair potential in a superconducting segment is Δ and we denote its zero temperature value by Δ_0. We assume that the superconducting segment is heavily doped so that the proximity effect induces superconductivity on graphene[15] (i.e., $U_0 \gg \Delta_0$). In superconducting segment, the wave functions are given by

$$\Psi_{S,e,\nu} = \frac{\check{\chi}}{\sqrt{2}} \begin{bmatrix} \nu u_0 \\ u_0 \\ \nu v_0 \\ v_0 \end{bmatrix} e^{i\nu p_0 x} f_q(y), \tag{6}$$

$$\Psi_{S,h,\nu} = \frac{\check{\chi}}{\sqrt{2}} \begin{bmatrix} -\nu u_0 \\ u_0 \\ -\nu v_0 \\ v_0 \end{bmatrix} e^{-i\nu p_0 x} f_q(y), \tag{7}$$

$$u_0 = \sqrt{\frac{1}{2}\left(1 + \frac{\Omega}{E}\right)}, \quad v_0 = \sqrt{\frac{1}{2}\left(1 - \frac{\Omega}{E}\right)}, \tag{8}$$

$$p_0 = \frac{U_0 + \mu}{v_F}\cos c_s + i\kappa_s, \quad \sin c_s = \frac{v_F q}{U_0 + \mu}, \tag{9}$$

$$\kappa_s = \frac{\Delta_0(U_0 + \mu)\sin\beta}{p_0 v_F^2}, \quad \cos\beta = \left|\frac{E}{\Delta_0}\right|, \tag{10}$$

$$\sin\beta = \begin{cases} \sqrt{1 - (E/\Delta_0)^2} & :|E| < \Delta_0 \\ -i\sqrt{(E/\Delta_0)^2 - 1} & :|E| > \Delta_0 \end{cases} \tag{11}$$

$$\check{\chi} = \begin{pmatrix} e^{i\varphi/2} & 0 & 0 & 0 \\ 0 & e^{i\varphi/2} & 0 & 0 \\ 0 & 0 & e^{-i\varphi/2} & 0 \\ 0 & 0 & 0 & e^{-i\varphi/2} \end{pmatrix}, \tag{12}$$

where $\Omega = \sqrt{E^2 - \Delta_0^2}$, φ is the phase of superconductor, $f_q(y)$ is the wave function in the y direction with a momentum q, $e(h)$ in the subscript of Ψ represents electron (hole) branch, and $\nu = 1$ or -1 indicates moving direction of a quasiparticle in the x direction. In a ferromagnetic segment, the wave function is described by

$$\Psi_{F,s,e,\nu} = \frac{1}{\sqrt{2}} \begin{bmatrix} e^{-i\nu a/2} \\ \nu e^{i\nu a/2} \\ 0 \\ 0 \end{bmatrix} e^{i\nu p_e x} f_q(y), \tag{13}$$

$$\Psi_{F,s,h,\nu} = \frac{1}{\sqrt{2}} \begin{bmatrix} 0 \\ 0 \\ -\nu e^{-i\nu b/2} \\ e^{i\nu b/2} \end{bmatrix} e^{i\nu p_h x} f_q(y), \tag{14}$$

$$\sin a = \frac{v_F q}{E + \mu + sV_{\rm ex}}, \quad p_e = \frac{E + \mu + sV_{\rm ex}}{v_F}\cos a, \tag{15}$$

$$\sin b = \frac{v_F q}{E - \mu + sV_{\rm ex}}, \quad p_h = \frac{E - \mu + sV_{\rm ex}}{v_F}\cos b. \tag{16}$$

The wave functions in the two segments are connected at the junction interface,

$$\Psi_{F,s,e,+} + r_{ee}\Psi_{F,s,e,-} + r_{he}\Psi_{F,s,h,-} = t_{ee}\Psi_{S,e,+} + t_{he}\Psi_{S,h,+}. \tag{17}$$

Here r_{ee} and r_{he} are, respectively, the normal and Andreev reflection coefficients at the interface with a ferromagnet. They have a form

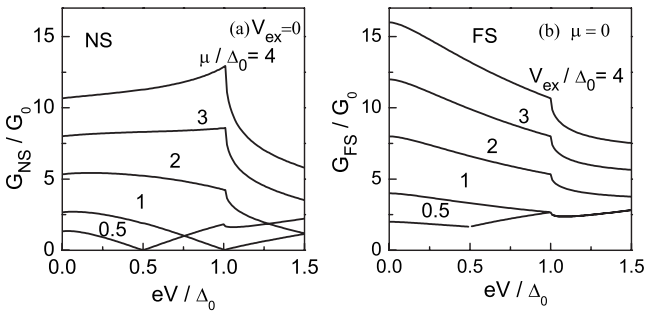

FIG. 2. Differential conductance of versus bias voltage. We choose $V_{ex}=0$ in (a) and $\mu=0$ in (b).

$$r_{he} = \cos a e^{-i\varphi}/X, \tag{18}$$

$$r_{ee} = i\left[\cos\beta \sin\left(\frac{a+b}{2}\right) + i \sin\beta \sin\left(\frac{a-b}{2}\right)\right] \Big/ X, \tag{19}$$

$$X = \cos\beta \cos\left(\frac{a-b}{2}\right) + i \sin\beta \cos\left(\frac{a+b}{2}\right). \tag{20}$$

The differential conductance of junction at zero temperature follows from the Blonder-Tinkham-Klapwijk[23] formula,

$$G_{FS} = \frac{2e^2}{h} \sum_{s=\pm 1} \sum_{q} [1 - |r_{ee}|^2 + |r_{he}|^2]_{s,E=eV}, \tag{21}$$

$$\sum_q \to \frac{N_s}{2} \int_{-\pi/2}^{\pi/2} da \cos a, \quad N_s = \frac{|\mu + eV + sV_{ex}|W}{\pi v_F}, \tag{22}$$

where N_s is the number of propagating channels of an incident electron. The number of propagating channels of outgoing hole is given by

$$M_s = \frac{|-\mu + eV + sV_{ex}|W}{\pi v_F}. \tag{23}$$

As is seen from the above expression, the conductance is expected to have some characteristic structure at such values of eV, which result in $N_s=0$ or $M_s=0$.

In Fig. 2, we show the conductance of FS junction as a function of bias voltages. The vertical axis is normalized by a constant value independent of μ and V_{ex}

$$G_0 = \frac{2e^2}{h} \frac{W}{\pi \xi_0}, \quad \xi_0 = \frac{v_F}{\Delta_0}. \tag{24}$$

We first summarize the conductance of NS junction[15] in Fig. 2(a), where $V_{ex}=0$. The conductance for $\mu/\Delta_0=0.5$ and that for $\mu/\Delta_0=1$, respectively, have bending structure at $eV=0.5\Delta_0$ and $eV=\Delta_0$ because $M_s=0$ holds at these points. The amplitude of conductance increases with the increase in μ for $\mu>\Delta_0$ because the number of propagating channels basically increases with μ. The conductance spectra are close to those in usual NS junctions with highly transparent interface. In graphene NS junctions, however, the Andreev reflection probability in the subgap region is always smaller than unity. Second, we focus on the conductance in the limit of $\mu\to 0$ as shown in Fig. 2(b). In usual metallic ferromagnets, $\mu \ll V_{ex}$ describes a half metal within the single-band picture. In a FS junction on a graphene, electronic structures are metallic for both spin directions because the conduction band is not limited from the bottom. When the Fermi energy of a spin-up electron lies on the upper cone, that of a spin-down electron is in the lower cone as shown in Fig. 3(a). The similar argument is also given by Ref. 24. The line shape of conductance spectra in Fig. 2(b) can be understood by the following argument. As shown in Fig. 3(b), a in Eq. (15) and b in Eq. (16) represent, respectively, an incident angle of an electron and a reflection angle of a hole. At $\mu=0$, the relation $a=b$ holds for all E and V_{ex}. As a result, the integral with respect to a in Eqs. (21) and (22) becomes independent of V_{ex}. Only N_s and M_s [Eqs. (22) and (23)] depend on V_{ex}. The differences in line shapes of conductance in Fig. 2(b) mainly come from the dependence of N_s and M_s on eV. At $V_{ex}=0.5\Delta_0$, $N_{s=1}$ increases with increasing eV. On the other hand, $N_{s=-1}$ first decreases to zero at $eV=V_{ex}$ then increases with increasing eV. Thus the conductance spectra show bending structure at $eV=V_{ex}$. For $V_{ex}>\Delta_0$, the line shape of conductance is independent of V_{ex} and the amplitude is simply proportional to V_{ex}. It should be noted that the Andreev reflection probability is unity at $eV=0$ for $V_{ex}>\Delta_0$. Therefore, according to Ref. 8, very small shot noise is expected near the zero bias. This feature remains unchanged as far as a relation $\mu \ll V_{ex}$ being satisfied.

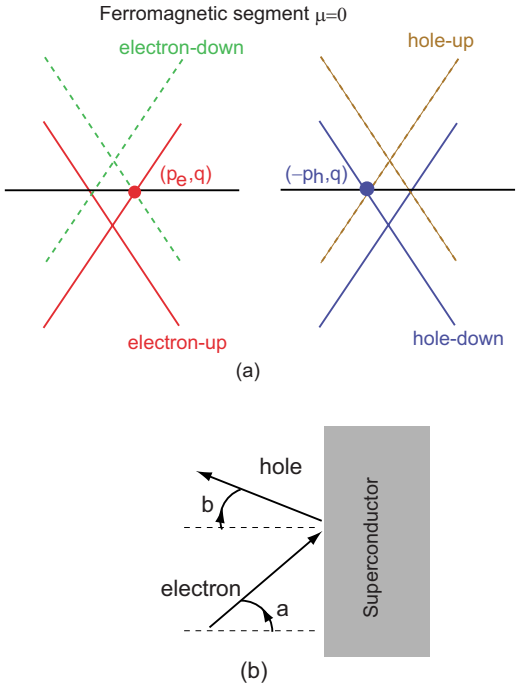

FIG. 3. (Color online) (a) The dispersion relation of a quasiparticle at $\mu=0$ in ferromagnetic segment. (b) Incident angle of an electron a and reflection angle of a hole b.

Here we briefly discuss the specular Andreev reflection in FS junction. The velocity of right moving incident electron is $v_F(\cos a, \sin a)$. On the other hand, the velocity of left moving hole is $v_F(-\cos b, \sin b)$. Since $a=b$ at $\mu=0$, the velocity component in the x direction changes its sign in the Andreev

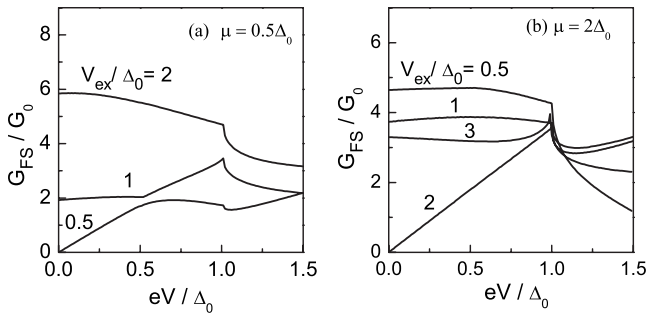

FIG. 4. Conductance spectra in FS junctions for $\mu=0.5\Delta_0$ in (a) and $\mu=2\Delta_0$ in (b).

reflection, whereas that in the y direction remains unchanged. Thus the Andreev reflection is always specular in a FS junction on graphene for $\mu \ll V_{\rm ex}$.

At $\mu=0.5\Delta_0$, the conductance spectra show more variety as seen in Fig. 4(a). At $V_{\rm ex}/\Delta_0=0.5$, the conductance at zero bias has very small value because the conditions $M_{s=1}=0$ and $N_{s=-1}=0$ are satisfied at $eV=0$. The conductance increases with increasing eV near zero bias because the bias voltage increases the number of propagating channels. For $V_{\rm ex}/\Delta_0=1$, the conductance has a bending structure at $eV=\mu$ because $N_{s=-1}$ becomes zero there. For $V_{\rm ex}=2\Delta_0$, the line shape of conductance is close to that of $V_{\rm ex}>\Delta_0$ in Fig. 2(b). In Fig. 4(b), we also show the conductance for $\mu=2\Delta_0$. At $V_{\rm ex}=0.5\Delta_0$, the conductance spectra are similar to those in NS junction in Fig. 2(a). The subgap conductance decreases with increase in $V_{\rm ex}$ as shown in Fig. 4(b) for the cases $V_{\rm ex}=\Delta_0$ and $V_{\rm ex}=2\Delta_0$. This is because the number of propagating channels decreases with increasing $V_{\rm ex}$. For $V_{\rm ex}>\mu$, the conductance spectra are close to those in Fig. 2(b).

In realistic junctions on graphene, the amplitude of pair potential Δ_0 would be expected to be on the order of 1 K. The constant slope of the dispersion relation $\hbar v_F$ is estimated to be 7×10^{-6} m K.[14] Thus the coherence length ξ_0 becomes on the order of 1 μm. The typical amplitude of the conductance is $(e^2/h)N_s$ with $N_s=W|\mu+eV+\pm V_{\rm ex}|/(\hbar v_F)$ being the number of propagating channels. When we choose W is about 1 μm, the conductance becomes the quantum conductance e^2/h for $|\mu+eV+\pm V_{\rm ex}|\simeq 1$ meV.

III. JOSEPHSON EFFECT IN SFS JUNCTIONS

Let us consider SFS junction as shown in Fig. 1(b), where we add a superconductor on the left-hand side of FS junction. We assume that the length of an insulator L is large enough so that the electric current through the insulator completely vanishes. Then the superconductors are electrically coupled only through the graphene sheet. The potentials of junctions in Eqs. (1) and (2) are replaced by

$$V(x)=\begin{cases}-U_0 & :x\le 0\\ 0 & :0<x<L\\ -U_0 & :x\ge L\end{cases}, \tag{25}$$

$$\Delta(x)=\begin{cases}\Delta e^{i\varphi_L} & :x\le 0\\ 0 & :0<x<L\\ \Delta e^{i\varphi_R} & :x\ge L\end{cases}. \tag{26}$$

The continuity equation of electron density implies

$$\partial_t n(\boldsymbol{r})+\nabla\cdot\boldsymbol{j}(\boldsymbol{r})=0, \tag{27}$$

$$\boldsymbol{j}(\boldsymbol{r})=\frac{-ev_F}{2}\sum_s T\sum_{\omega_n}\times \mathrm{Tr}\left[\begin{pmatrix}\hat{\boldsymbol{\sigma}} & \hat{0}\\ \hat{0} & \hat{\boldsymbol{\sigma}}\end{pmatrix}\check{\boldsymbol{G}}^{(s)}(\boldsymbol{r},\boldsymbol{r},\omega_n)\right], \tag{28}$$

where $\check{\boldsymbol{G}}^{(s)}$ is the Matsubara-Green function of SFS junction at $\boldsymbol{r}=(x,y)$ with $0\le x\le L$ and $\omega_n=(2n+1)\pi T$ is the Matsubara frequency with n and T being an integer number and a temperature, respectively. The trace is carried out over Nambu and sublattice spaces. The Josephson current in SFS junction is obtained by integrating Eq. (28) with respect to y. In direct-current Josephson effect, the Josephson current does not depend on x. Thus we choose $x=0$ in what follows. Without losing generality, we obtain the total Josephson current in SFS junctions,

$$J=\frac{e}{2\hbar}\sum_{s=\pm1}\sum_q T\sum_{\omega_n}\frac{\Delta}{\Omega_n}[r_{he}-r_{eh}]_s, \tag{29}$$

where $\Omega_n=\sqrt{\omega_n^2+\Delta^2}$. For propagating channels, the summation is replaced by

$$\sum_q \to \frac{N_s}{2}\int_{-\pi/2}^{\pi/2} da\cos a, \quad N_s=\frac{|\mu+sV_{\rm ex}|W}{\pi v_F}. \tag{30}$$

The current expression coincides with Furusaki-Tsukada formula.[25,26] In Eq. (29), r_{eh} and r_{he} are the Andreev reflection coefficients, which should be calculated in an SFS junction. From appropriate boundary condition at $x=0$ and L, they become

$$[r_{he}-r_{eh}]_{s=1}=\Delta\Omega_n D\Xi, \tag{31}$$

$$\Xi=\frac{A\omega_n^2+\Delta^2 R}{P\omega_n^4+\omega_n^2\Delta^2 Q+\Delta^4 R^2}, \tag{32}$$

$$P=A^2+C^2, \quad Q=(2RA+C^2), \tag{33}$$

$$R=(A+B+D\cos\varphi)/2, \tag{34}$$

with φ being the phase difference between the two superconductors, and

$$A=\cos(p_eL)\cos a\cos(p_hL)\cos b-\sin(p_eL)\sin(p_hL), \tag{35}$$

$$B=\sin(p_eL)\sin a\sin(p_eL)\sin b, \tag{36}$$

$$C=\cos(p_eL)\cos a\sin(p_hL)+\cos(p_hL)\cos b\sin(p_eL), \tag{37}$$

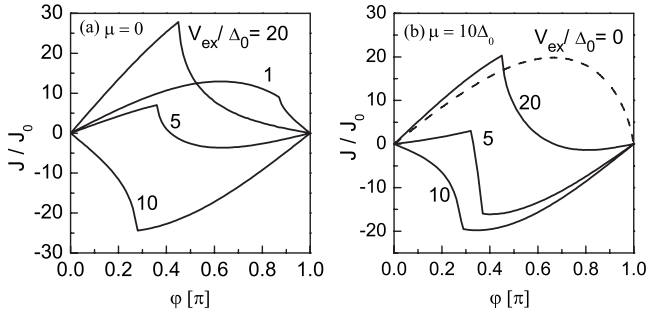

FIG. 5. Current-phase relation of SFS junction at $T=0$ for $\mu=0$ in (a) and $\mu=10\Delta_0$ in (b).

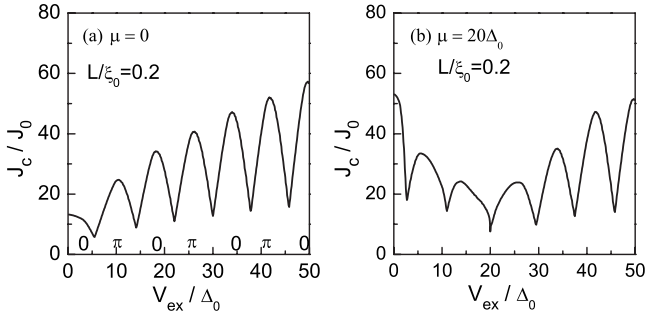

FIG. 6. Critical Josephson current versus exchange potential at $T=0$ and $L=0.2\xi_0$.

$$D = \cos a \cos b. \tag{38}$$

Here a, b, p_e, and p_h are given by Eqs. (15) and (16) with $E\to 0$. The results for $s=-1$ are obtained by $V_{\rm ex}\to -V_{\rm ex}$ in above results. For short junctions $L \ll \xi_0 = v_F/\Delta_0$, we obtain

$$J = e\sum_{s=\pm 1}\sum_{q}\frac{\sin\varphi D}{\sqrt{Q^2-4PR^2}}\times\left[\frac{\omega_+^2 A - R\Delta^2}{\omega_+}\tanh\left(\frac{\omega_+}{2T}\right) - \frac{\omega_-^2 A - R\Delta^2}{\omega_-}\tanh\left(\frac{\omega_-}{2T}\right)\right], \tag{39}$$

where $\omega_\pm^2 = \Delta^2(Q \pm \sqrt{Q^2-4PR^2})/2P$. At $V_{\rm ex}=0$, we recover the previous results for SNS junction.[27]

In Fig. 5, we show current-phase relation (CPR) of SFS junction at $T=0$ for $\mu=0$ in Fig. 5(a) and $\mu=10\Delta_0$ in Fig. 5(b), where we choose $L=0.2\xi_0$. The vertical axis is normalized by a constant value of $J_0=e\Delta_0 W/\pi\xi_0$, which is independent of μ and $V_{\rm ex}$, and is about 0.01 μA for $W=1$ μm and $\Delta_0=1$ K. We first pay attention to the CPR in SNS junction,[27] which is represented by a broken line in Fig. 5(b). In SNS junctions, the Josephson current has a CPR, which slightly deviates from the sinusoidal relation for $\mu \gg \Delta_0$. On the other hand in SFS junction, the CPR shows complicated structures depending on $V_{\rm ex}$, as shown in Fig. 5(a). At $V_{\rm ex}=\Delta_0$, the Josephson current mainly flows through evanescent channels and CPR is similar to that in the short diffusive SNS junction.[27] At $V_{\rm ex}=5\Delta_0$, the contribution of propagating channel dominates the Josephson current, and the CPR suddenly deviates from a linear relation around the critical phase difference $\varphi=0.35\pi$. In the limit of $\mu=0$, the Josephson current at $T=0$ becomes

$$J = e\Delta_0\cos(\varphi/2)\sum_q T\sum_{\omega_n}\frac{|\omega_+|-|\omega_-|}{2\Delta_0 b_s c_s\cos(p_e L)} \times[(1-2c_s^2)+\mathrm{sgn}\{\cos^2(p_e L)-\sin^2(\varphi/2)\}], \tag{40}$$

with

$$b_s = \sqrt{1 - T_n \sin^2(\varphi/2)}, \tag{41}$$

$$c_s = \sqrt{1 - T_n \cos^2(p_e L)}, \tag{42}$$

$$T_n = \frac{\cos^2 a}{\cos^2 a \cos^2(p_e L) + \sin^2(p_e L)}, \tag{43}$$

$$\omega_\pm = \Delta_0\sqrt{T_n}[b_s\cos(p_e L) \pm c_s \sin(\varphi/2)]. \tag{44}$$

The energies of the bound states are given by $\pm\omega_\pm$. For $\varphi>0$ and $p_e L \lesssim 1$, ω_- changes its sign at φ_c, satisfying $\cos^2(p_e L)-\sin^2(\varphi_c/2)=0$. Namely, the two Andreev bound states $\pm\omega_-$ go across the Fermi level at φ_c. As a result, the Josephson current changes its sign. The transition is not so sharp because φ_c depends on an incident angle of a quasiparticle. This situation is similar to the $0-\pi$ transition in diffusive superconductor/ferromagnet/constriction/ferromagnet/superconductor junction.[7] Although SFS junctions on graphene is free from impurity scatterings, it shows a characteristic property of diffusive junctions. The Josephson current are always negative and positive for all $\varphi>0$ at $V_{\rm ex}=10\Delta_0$ and $20\Delta_0$, respectively. This tendency can be also observed even in the presence of μ as shown in Fig. 5(b) with $\mu=10\Delta_0$.

The Josephson current oscillates as a function of $V_{\rm ex}$ as shown in Fig. 6. At $\mu=0$ in Fig. 6(a), the amplitude of critical current totally increases with the increase in $V_{\rm ex}$ because the number of propagating channels increases with increasing $V_{\rm ex}$. At the same time, the critical current shows oscillations, which indicate the $0-\pi$ transition. Strictly speaking, the oscillations are not identical to the $0-\pi$ transition in usual SFS junctions because the CPR deviates far from the sinusoidal relation. In Fig. 6, we first calculate the CPR for fixed $V_{\rm ex}$ in $0<\varphi<\pi$ then determine the critical current. If the critical current flows to the $+x$ direction, we assign such junction as 0 junction in Fig. 6. In the same way, if the critical current flows to the $-x$ direction, we label such junction as π junction. At the $0-\pi$ transition points, the critical current still have a large value because of the higher harmonics.[28] At $V_{\rm ex}=0$, the critical current does not become zero because the contribution of the evanescent channels makes the Josephson current a finite value.

For $\mu=20\Delta_0$, as shown in Fig. 6(b), the amplitude of the critical current first decreases with increasing $V_{\rm ex}$ then increases. At $V_{\rm ex}=\mu$, the critical current becomes a small value because the number of propagating channels becomes zero. The Josephson coupling through the evanescent channels gives a finite critical current there. We analytically confirm that the junction is always in the 0 state in the limit of $V_{\rm ex}=0$.

In Fig. 7(a), we show the critical current at $\mu=0$ and $T=0$, where we choose $L=0.1\xi_0$ and $0.5\xi_0$. With Fig. 6(a), we

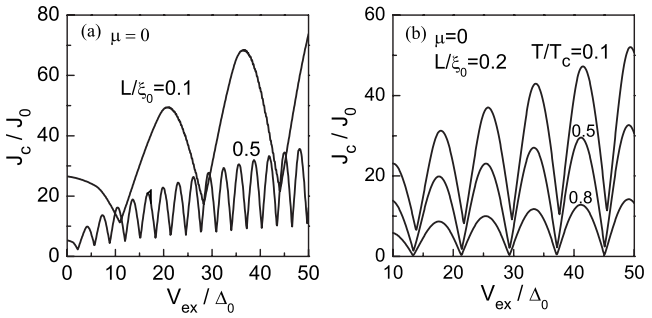

FIG. 7. Critical Josephson current versus exchange potential at $T=0$ for $L=0.2\xi_0$ and $0.5\xi_0$ in (a). Critical Josephson current is shown for several choices of temperature for $L=0.2\xi_0$ in (b).

find that the period of oscillations becomes shorter for larger L. At the same time, the amplitude of the critical current becomes smaller for larger L. Figure 7(b) shows the critical current for $L=0.2\xi_0$ for several choices of temperatures: $T/T_c=0.1$, 0.5, and 0.8 from top to bottom. The $0-\pi$ transition points remain almost unchanged at finite temperatures. Thus $0-\pi$ transition by changing temperature is absent in SFS junctions on graphene, as well as in usual SFS junction in the clean limit.[7]

IV. CONCLUSION

We have studied electron transport in ferromagnet-superconductor (FS) junctions and superconductor-ferromagnet-superconductor (SFS) on graphene. Cooper pairs can carry electric current even when exchange potential (V_{ex}) is much larger than the Fermi energy (μ) in a ferromagnet because electric structures of graphene lose a bottom. The exchange potential rather enhances the electron transport on graphene. The Andreev reflection is always specular reflective for $\mu=0$. As a consequence, the line shape of conductance spectra in FS junctions is independent of V_{ex} for sufficiently large V_{ex}. In addition, the Andreev reflection probability at the zero bias is unity, which leads to small shot noise near the zero bias. In SFS junction, the Josephson current shows complicated current-phase relationships. The SFS junction exhibits the $0-\pi$ transition behavior as changing V_{ex}.

ACKNOWLEDGMENTS

This work was partially supported by the Dutch FOM, the NanoNed program under Grant No. TCS7029 and Grant-in-Aid for Scientific Research from The Ministry of Education, Culture, Sports, Science and Technology of Japan (Grants No. 17071007, No. 19540352, and No. 20029001).

[1] P. Fulde and R. A. Ferrell, Phys. Rev. **135**, A550 (1964).
[2] A. I. Larkin and Y. N. Ovchinnikov, Sov. Phys. JETP **20**, 762 (1965).
[3] A. I. Buzdin, L. N. Bulaevskii, and S. V. Panyukov, JETP Lett. **35**, 179 (1982).
[4] A. I. Buzdin, Rev. Mod. Phys. **77**, 935 (2005).
[5] V. V. Ryazanov, V. A. Oboznov, A. Yu. Rusanov, A. V. Veretennikov, A. A. Golubov, and J. Aarts, Phys. Rev. Lett. **86**, 2427 (2001).
[6] T. Kontos, M. Aprili, J. Lesueur, F. Genet, B. Stephanidis, and R. Boursier, Phys. Rev. Lett. **89**, 137007 (2002).
[7] A. A. Golubov, M. Yu. Kupriyanov, and E. I'ichev, Rev. Mod. Phys. **76**, 411 (2004).
[8] M. J. M. de Jong and C. W. J. Beenakker, Phys. Rev. Lett. **74**, 1657 (1995).
[9] R. S. Keizer, S. T. B. Goennenwein, T. M. Klapwijk, G. Miao, G. Xiao, and A. Gupta, Nature (London) **439**, 825 (2006).
[10] M. Eschrig, J. Kopu, J. C. Cuevas, and G. Schon, Phys. Rev. Lett. **90**, 137003 (2003).
[11] Y. Asano, Y. Tanaka, and A. A. Golubov, Phys. Rev. Lett. **98**, 107002 (2007).
[12] V. Braude and Yu. V. Nazarov, Phys. Rev. Lett. **98**, 077003 (2007).
[13] M. Eschrig and T. Lofwander, Nat. Phys. **4**, 138 (2008).
[14] T. Ando, J. Phys. Soc. Jpn. **74**, 777 (2005).
[15] C. W. J. Beenakker, Phys. Rev. Lett. **97**, 067007 (2006).
[16] D. Greenbaum, S. Das, G. Schwiete, and P. G. Silvestrov, Phys. Rev. B **75**, 195437 (2007).
[17] N. M. R. Peres, F. Guinea, and A. H. Castro Neto, Phys. Rev. B **72**, 174406 (2005).
[18] Y.-W. Son, M. L. Cohen, and S. G. Louie, Nature (London) **444**, 347 (2006).
[19] P. M. Tedrow, J. E. Tkaczyk, and A. Kumar, Phys. Rev. Lett. **56**, 1746 (1986).
[20] H. Haugen, D. Huertas-Hernando, and A. Brataas, Phys. Rev. B **77**, 115406 (2008).
[21] Y. G. Semenov, K. W. Kim, and J. M. Zavada, Appl. Phys. Lett. **91**, 153105 (2007).
[22] N. Tombros, C. Jozsa, M. Popinciuc, H. T. Jonkman, and B. J. van Wees, Nature (London) **448**, 571 (2007).
[23] G. E. Blonder, M. Tinkham, and T. M. Klapwijk, Phys. Rev. B **25**, 4515 (1982).
[24] M. Zareyan, H. Mohammadpour, and A. G. Moghaddam, arXiv:0804.2774 (unpublished).
[25] A. Furusaki and M. Tsukada, Solid State Commun. **78**, 299 (1991).
[26] Y. Asano, Phys. Rev. B **64**, 224515 (2001).
[27] M. Titov and C. W. J. Beenakker, Phys. Rev. B **74**, 041401(R) (2006).
[28] J. Linder, T. Yokoyama, D. Huertas-Hernando, and A. Sudbo, Phys. Rev. Lett. **100**, 187004 (2008).